ELSEVIER

Contents lists available at ScienceDirect

## **Engineering Geology**

journal homepage: www.elsevier.com/locate/enggeo



## Check for updates

# Spatiotemporal characteristics of discontinuous soil failures on debris flow source slopes

Xiaojun Guo<sup>a,b</sup>, Yong Li<sup>a,\*</sup>, Peng Cui<sup>a,b</sup>, Yan Yan<sup>c</sup>, Baoliang Wang<sup>d</sup>, Jun Zhang<sup>e</sup>

- a Kev Laboratory of Mountain Hazards and Surface Process/Institute of Mountain Hazards and Environment. Chinese Academy of Sciences. Chenedu 610041. China
- <sup>b</sup> CAS Center for Excellence in Tibetan Plateau Earth Sciences, Beijing 100101, China
- <sup>c</sup> School of Civil Engineering, Southwest Jiaotong University, Chengdu 610031, China
- <sup>d</sup> Yellow River Engineering Consulting Co., Ltd., Zhengzhou 450004, China
- e University of Chinese Academy of Sciences, Beijing 100049, China

#### ARTICLE INFO

## Keywords: Slope failure Rainfall intensity Grain size distribution Soil heterogeneity Time series

#### ABSTRACT

Slope failures represent important supplies of material for debris flows, and field observations have indicated that failures across a slope are random and discontinuous. However, few studies have focused on the nature of successive failures. This study conducted field experiments on soil failure under artificial rainfall on slopes in two typical debris flow valleys, and established the random nature of the failure sequence that comprises a slope process. It was found that failures occur separately and intermittently on slopes. Furthermore, failure sequences under different rainfall and slope conditions have certain characteristics in common: 1) a failure sequence that comprises primarily random uncorrelated individual failures is independent of rainfall conditions; 2) the time interval between failures satisfies an exponential distribution, and the average length of the interval decreases with increasing rainfall intensity; and 3) the magnitude of failure fluctuates by up to three orders, from several to hundreds of volume units  $(10^{-3} \text{ m}^3)$ , and the distribution follows a power law whereby the total amount increases with increasing rainfall intensity. We propose that these properties are ascribed to the spatial heteroseneity of the soil, which can be described by the grain size distribution (GSD). The variation of GSD parameters across a slope determines the randomness, intermittency, and fluctuation of shallow failures. These findings support the development of scenarios for the occurrence of intermittent debris flow surges supplied by random failure sequences.

## 1. Introduction

Shallow slope failures induced by rainfall are important providers of material for debris flows (Guo et al., 2020). Such failures, which are usually small and occur independently and randomly on slopes, differ considerably from larger landslides. Therefore conventional methods used for analysis of slope stability, which are focused primarily on determining the variation of safety factors across a slope and identifying a potential slip surface (e.g., Xiao et al., 2018; Feng et al., 2019), cannot be applied to shallow failures scattered across a slope with no slip surface. In relation to debris flows, shallow slope failures provide a discontinuous and random supply of material that can ultimately result in separate successive mainstream surges (Guo et al., 2020). The critical characteristics of such a slope process are the behavior and spatiotemporal features of the collective failures rather than those of any

individual event. Therefore, this requires consideration of a scenario of failures over a slope where the soil has high spatial variability and intrinsic uncertainty (Vanmarcke, 1977, 1980, 1983; Phoon and Kulhawy, 1999; Mori et al., 2020; Baecher and Christian, 2005; Uzielli et al., 2005).

Although slope stability analysis generally uses multiple elements to predict a single slope failure, this study addressed the case in which a slope produces various failures under given soil and rainfall conditions. In this paper, we report on a series of artificial rainfall experiments on slopes in debris flow source areas that revealed the spatial patterns and temporal sequences of shallow slope failures. Then, we establish similar statistical characteristics of failure sequences under different rainfall conditions, and propose a probabilistic mechanism for progressive failures using random granular features of the soils. The findings support the development of a comprehensive scenario of progressive shallow

<sup>\*</sup> Corresponding author.

E-mail address: ylie@imde.ac.cn (Y. Li).

failures across soil slopes.

## 2. Background and experiment setting

## 2.1. General purpose and methodologies

The objective of this study was to seek a comprehensive scenario of multiple failures on soil slopes that feed debris flows. To establish the universality of the scenario, we conducted experiments on slopes in two gullies with different geological and geomorphological circumstances in Southwest China. Because failures observed in the field display properties of high discreteness and randomness, only a statistical scenario is achievable at present. Moreover, in the statistical sense, the reproducibility of the experiments relies on the statistical characteristics of failures across a slope rather than on similarity with any single failure. Therefore, we performed time series analysis to explore and compare the temporal features of the failure sequences. Specifically, we calculated Pearson, Kendall, and Spearman coefficients (Fieller et al., 1957; Kendall and Stuart, 1983) to establish the strength of the correlation between the magnitude and time interval of the failures, and we used the Hurst exponent (Hurst et al., 1965; McCauley et al., 2007) with the Augmented Dickey-Fuller test and the Mann-Kendall Trend test to determine the autocorrelation of the failure sequence. Both tests can indicate whether successive failures have high randomness. Then, we established the power law magnitude-frequency relationship and the exponential distribution of the time interval for failures under different conditions, which are factors that describe the spatial and temporal characteristics of failure sequences. Correspondingly, we did not seek the mechanism of progressively separate failures; instead, we employed random granular features of the soil that determine the potentiality of failure under different rainfall intensities to provide a probabilistic basis for the mechanism of progressive failures.

## 2.2. Experimental settings

The experiments were conducted on the slopes of two debris flow gullies in Southwest China: the Jiangjia Gully (JJG) in Yunnan Province and the Niujuan Gully (NJG) in Sichuan Province. JJG is known for the high frequency and variability of its debris flows (e.g., Cui et al., 2005;

Guo et al., 2016a, 2020), and NJG was affected severely by the Ms. 8.0 Wenchuan earthquake that occurred on May 12, 2008 (Fig. 1). Focusing on slope failures as providers of material for debris flows, the experimental locations were selected according to three criteria: 1) the gullies have frequent debris flows and distinctive geomorphological and climatic characteristics that represent a wide spectrum of environmental conditions, 2) the slopes represent a source of material for debris flows, and 3) the source material is representative of the general soil conditions.

The JJG is covered with colluvium that has a wide-ranging grain size distribution (GSD). Approximately 80% of the outcrops are weak and easily weathered. Landslide deposits of various scale with slope gradient of between  $30^\circ$  and  $40^\circ$  are distributed throughout the valley. Shallow failures are the main providers of material to debris flows (e.g., Cui et al., 2005). Since the occurrence of the 2008 Wenchuan earthquake, the NJG has been prone to frequent debris flows (e.g., Guo et al., 2016b). The basic geographic parameters of the two gullies are listed in Table 1. The slopes are dominated by gradient of  $30^\circ-32^\circ$ , and the experiment fields encompassed areas of  $8\times 4$  m.

We used an artificial device comprising a water pump and sprayers to simulate the natural rainfall that triggers slope failures. The artificial rainfall was generated using water drawn from the gully by the pump. Adjustment of the water pressure and sprayer size regulated the rainfall intensity ( $I_R$ ). The device provided rainfall over an area 4-m deep and 8-m wide. In accordance with known local rainfall conditions (Guo et al., 2016b, 2020), we set seven values for  $I_R$  in the JJG experiments (i.e., 12, 18, 27, 36, 45, 54, and 60 mm/h) and six values for  $I_R$  in the NJG experiments (i.e., 18, 25, 35, 45, 70, and 80 mm/h). The duration of each experiment was 40 min.

**Table 1**Brief geographic parameters of two selected valleys.

Ravines	Area (km²)	Average slope (°)	Difference of Elevation (m)	Annual rainfall (mm)	Major rocks
Jiangjia	48.6	32	2227	600-1200	Phyllite
Niujuan	10.5	31	1833	1250	Granite and diorite

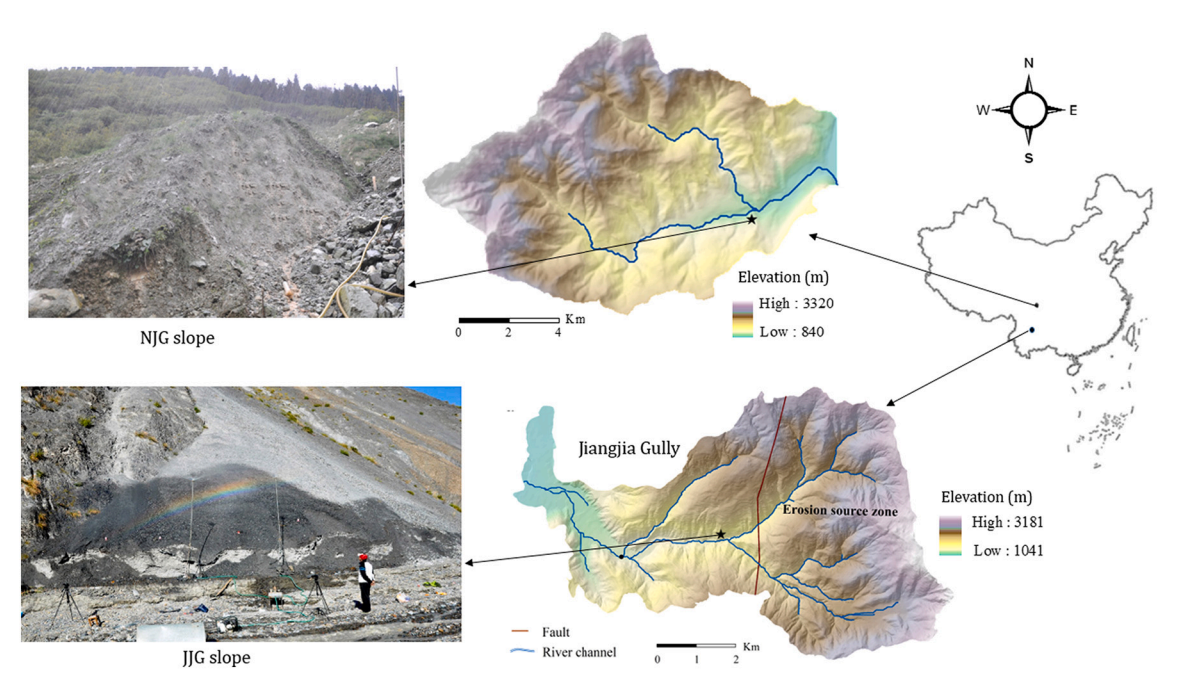


Fig. 1. Locations of the gullies and slopes used in the experiments.

#### 2.3. Soil conditions

The soil on each of the two slopes has distinct characteristics (Fig. 2). In JJG, the loose deposits consist primarily of weathered phyllite, whereas in NJG they are mainly granite and diorite. The JJG slope has highly coarse-grained particles and is virtually free of clay content (<0.002 mm); the content of fine grains (<0.075 mm) is only 0.5%–1.5% (average: 1.2%). The average content of fine grains on the NJG slope is 6.3%.

The grain composition of soil can be well described by the scaling GSD (Li et al., 2013, 2017):

$$P(\rangle D) = CD^{-\mu} \exp(-D/D_c) \tag{1}$$

where P(>D) is the cumulative fraction of grains with size greater than D, C is a coefficient, and  $\mu$  and  $D_c$  are the characteristic exponent and size, respectively. All these parameters can be obtained directly by fitting a curve to the frequency distribution of grain size using standard granulometric analysis (Table 2). Because C is a certain function of  $\mu$ , the GSD reduces to two parameters:  $\mu$  and  $D_c$ .

Generally, given the grain size range,  $\mu$  increases with the content of fine particles, whereas  $D_c$  increases with the upper limit of grain size. However, the high value of  $\mu$  in JJG cannot be compared with that in NJG owing to the effect of the lower limit of grain size, as shown in Fig. 2, i.e., 0.075 mm in JJG and 0.001 mm in NJG (Li et al., 2017). If we correct the GSD of NJG using the same size range, the average value of  $\mu$  would be 0.065, i.e., higher than that in JJG. In summary, the material comprising the JJG slope is much coarser than that of the NJG slope, which sets the background of the material involved in the slope processes. It is also noted that even within the small areas of the experiments, the grain composition varied markedly, as indicated by the GSD parameters, highlighting the importance of the spatial heterogeneity of soil regarding the behavior of slope failures.

## 2.4. Experimental procedure and data processing

The objective was to find an overall scenario of soil failure on slopes under different soil and rainfall conditions; therefore, we ran experiments on both the JJG slope and the NJG slope under the set rainfall intensities. After each experiment, we allowed an interval of several days for the slope moisture to recover its usual state. Before running an experiment, we measured the average initial moisture conditions of the slope soil to ensure that it was within the range of 8%–12%. This guaranteed comparability between the effects of the various rainfall

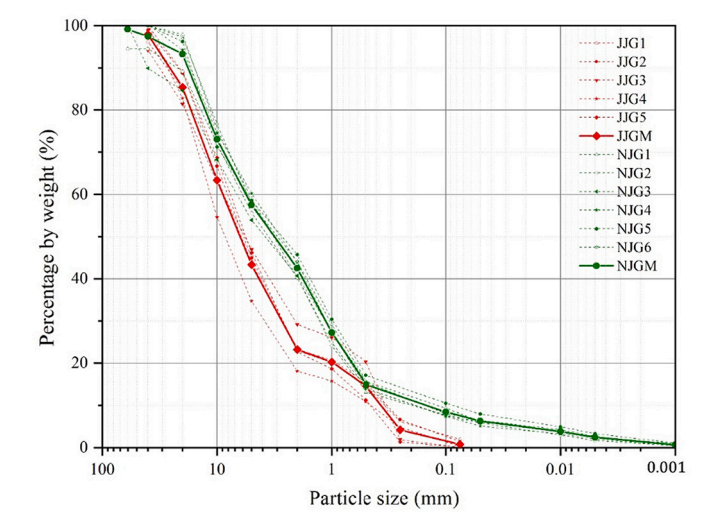


**Fig. 2.** Grain composition of each of the experimental slopes (JJGM and NJGM represent the mean (i.e., the mixture) grain composition of the soil samples).

**Table 2**Comparison of grain composition of soils of the test slopes.

Ravines	Samples	GSD parameters						
		С	μ	$D_{\rm c}$	$R^2$			
	1	92.11	0.01341	13.36	0.9968			
	2	85.62	0.01733	13.66	0.996			
NIIO	3	86.32	0.02642	20.76	0.9857			
NJG	4	90.83	0.01752	13.59	0.9931			
	5	86.49	0.02461	15.24	0.9906			
	6	89.27	0.01936	13.61	0.9948			
	1	89.01	0.0389	12.44	0.9973			
	2	90.15	0.0328	10.78	0.9958			
JJG	3	91.79	0.08677	16.8	0.9895			
	4	95.04	0.01819	13.17	0.9926			
	5	93.38	0.0322	9.94	0.9971			

intensities because the action of rainfall on the soil incorporated the component attributable to existing moisture.

Strictly, the running of individual experiments changed the slope conditions; however, each shallow failure removed only a small volume of material from the slope, and the geometry of the entire slope remained largely unchanged, especially considering the intrinsic irregularity of the topography. The point at issue is the collective properties of multiple failures across the slope, irrespective of the variability of the slopes. We expected to determine similar statistical features of the failure sequences that occurred on the two slopes. For this purpose, we recorded the time, location, and size of each failure in each experiment under a given rainfall intensity. The entirety of each experiment was recorded by video and analyzed using the trace projection transformation method to determine the time, location, and size of each successive failure. The trace projection transformation method is a combination of dense optical flow and perspective projection transformation, which allows quantitative analysis of soil motion through video obtained at various angles (Yan et al., 2016). The algorithm for interpreting and processing the data is implemented in C++ and realized in Visual Studio. To ensure reliability, data were also obtained by direct inspection of snapshots in combination with field observations. A grid with cell resolution of  $1 \times 1$  m was set on a video snapshot as a coordinate system. Each failure could be located in a cell grid and its size estimated through comparison with the reference failure body (10<sup>-3</sup> m<sup>3</sup>). Thus, the failure time and location could be read directly and the size of the failure estimated through comparison with the reference body. Comparison of data obtained by visual inspection (A) and by image interpretation (B), shown in Fig. 3, reveals a difference as small as

Each experiment resulted in a sequence of failures and the failures resulted in successive surges in the channel flow. Although occurring on a small scale, the failures could be considered representative of real processes on soil slopes in natural conditions because they occurred on real slopes under rainfall conditions appropriate for the locality. Thus, they were more realistic than failures obtained in laboratory experiments using a limited volume of soil.

## 3. Observations of the failure processes

## 3.1. Failure types

"Failure" is a general term that encompasses various shallow soil movements and the displacement of detached soil bodies (e.g., Varnes, 1978; Hungr et al., 2014). Experiment has identified three types of failure: collapses, slides, and surface rill erosion, which broadly correspond to the traditional classification of falling, sliding, and slope rill erosion.

## 3.1.1. Collapses

Collapse refers to the falling of soil as an aggregate of granular

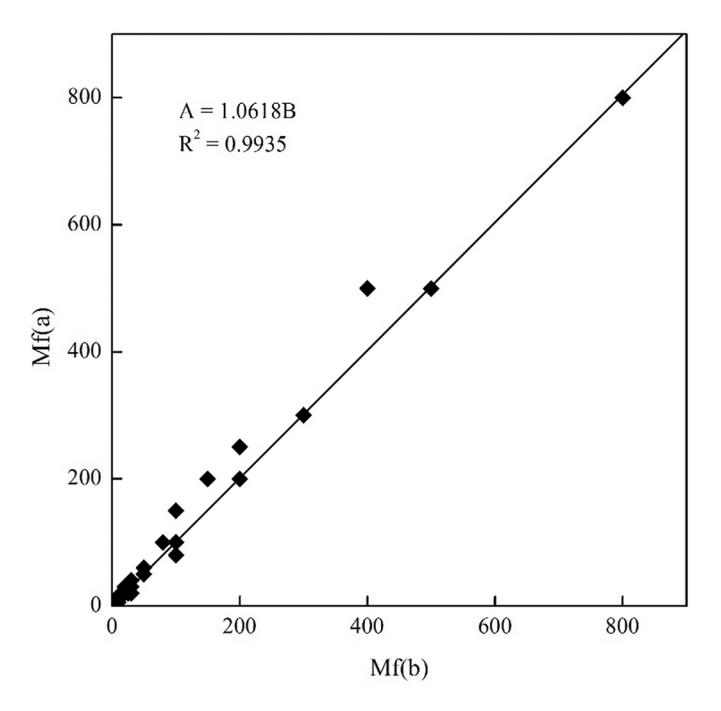


**Fig. 3.** Comparison of data obtained by visual inspection and by image interpretation (Mf denotes the failure magnitude).

material, which differs from a rockfall as a rigid body. Collapses on a slope are similar to those of a cohesionless sandpile, i.e., they fall downward like "fragmented rocks" freely rolling or falling on and off the slope at high velocity, simply driven by gravity and without soil–water interaction or destruction of soil structures. They occur individually or in clusters scattered across a slope and have size no greater than 30  $(10^{-3} \text{ m}^3)$ . Collapses occurred in all our experiments and represented

the majority in terms of the number of all types of failure; however, they contributed only a small proportion of the total volume.

#### 3.1.2. Slides

Here, slide is taken to mean movement of soil detached from the slope owing to destruction of the soil structure. Slides occur following rainfall infiltration and massive slides usually follow previous smaller failures. They form as a cascading process from the slope toe to upper locations (i.e., from A to D in Fig. 4). Slides differ from collapses in that they move en masse and move a definite distance on the slope surface with velocity of no more than 0.5 m/s. They are accompanied by obvious soil destruction and occur only under high-intensity rainfall (e. g.,  $I_{\rm R} > 27$  mm/h in JJG and  $I_{\rm R} > 45$  mm/h in NJG). Slides, which usually comprise layers of material several centimeters thick, can reach volumes that are substantially larger than those of collapses. Thus, they are dominant in slope processes and account for the majority of failure volume, e.g., approximately 83% of the total volume in experiment J-7.

#### 3.1.3. Rill erosion

Surface rill erosion appears similar to a fluidized debris avalanche (Sharpe, 1938; Hungr et al., 2014), which is actually a debris flow on an open slope. Flows on a slope develop rill erosion and initiate successive failures along the rill. Rill erosion begins with water incision that cuts through a "soft route" on the slope and excavates a rill (Fig. 5). Then, successive failures develop along the rill and combine with the rill flow. Rill erosion and flow occur mainly in NJG under high-intensity rainfall, e.g., 70 and 80 mm/h. It was found to occur at certain locations in both experiments.

## 3.2. Occurrence of various failures

To describe the details of the occurrence of a failure sequence, we consider the experiment conducted with rainfall intensity of 60 mm/h in JJG (i.e., experiment J-7), which not only presents a complete scenario of a slope process, but also reveals differences in the characteristics of

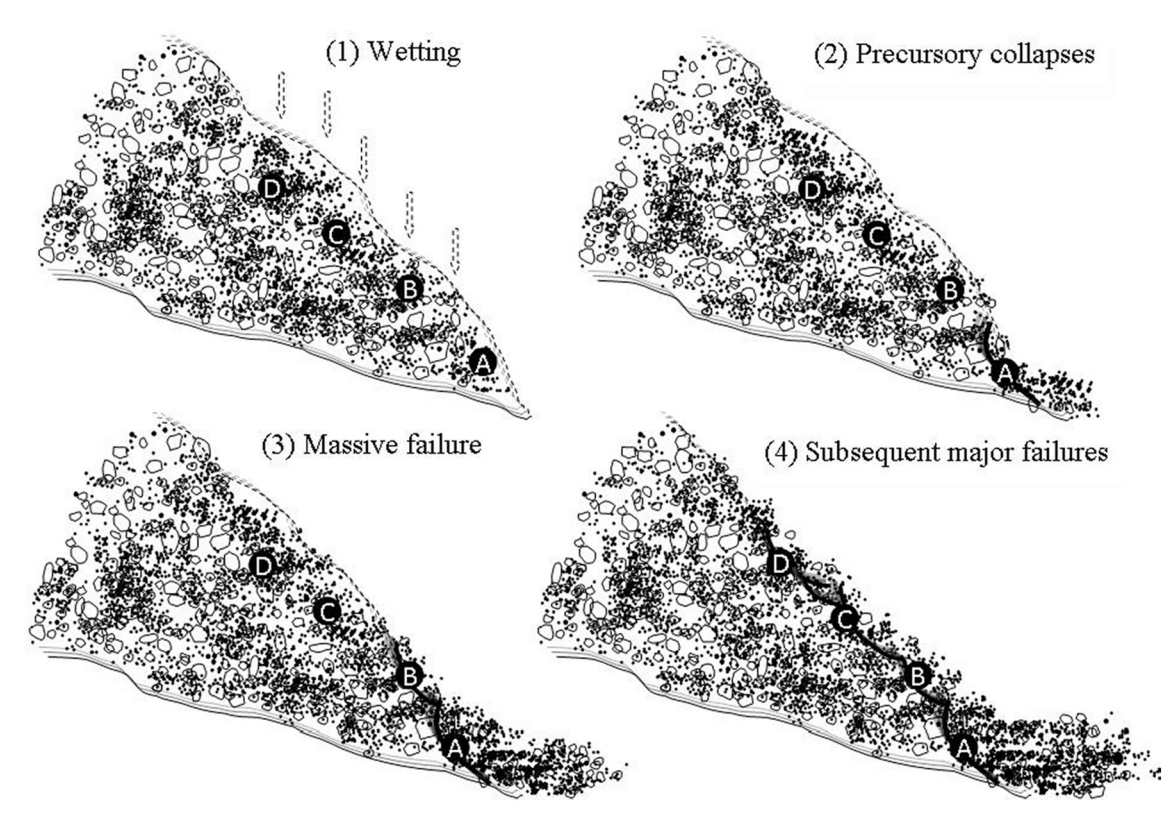


Fig. 4. Cascading slides on the slope in experiment J-7 in JJG.

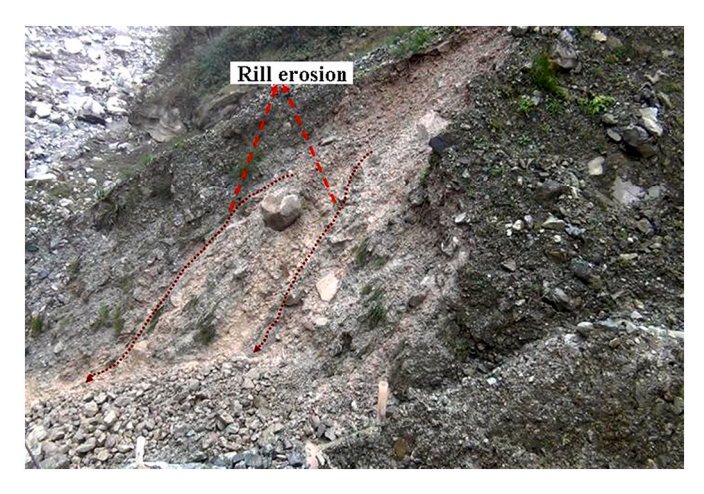


Fig. 5. Evidence of surface flow and rill erosion.

the failures owing to the heterogeneity of the soil. As shown in Fig. 6, the slope can be divided naturally into two parts (R1 and R2) on the basis of fine- and coarse-grained surface material, the GSD parameters of which are listed in Table 3.

Fig. 7 displays the distribution of failures on the slope observed in experiment J-7. The black dots indicate collapse locations, and the dot size represents the volume of the failure. The ellipses represent the scope of the slides, and the number pairs (n, M) denote that the n-th failure had magnitude of M (unit:  $10^{-3}$  m³). For example, (153, 500) means that failure No.153 occurred in the area shown and had a volume of 500  $(10^{-3}$  m³). The figure also shows the progression of slope failures from a single initial collapse on the slope toe to a subsequent massive failure above, followed by successive major failures in adjacent areas. During the 40-min duration of the experiment, 222 failures occurred of which 14 large failures (slides) contributed 83% of the total failure volume.

The distribution of the locations of the failures in space and time is remarkable. The first failure occurred at location (2,1) (here, the number pair (2, 1) is the coordinate of the failure location shown in Fig. 7). After 3 min 24 s, a subsequent failure occurred at a neighboring location (3,1). This was followed by three further successive failures at (3,1,3,2,3,3), which occurred between 3 min 24 s and 22 min 09 s, followed by three additional failures in neighboring regions. A similar process began at 11 m 30 s at location (7, 1, 7, 2) that resulted in another failure approximately 7 min later. Then, the slope developed a stable state and failures stopped for more than 10 min.

The slope activity "revived" at 30 min 09 s, when 4 large failures (slides) and more than 30 collapses occurred in a small area within 4 mins (in the red square shown in Fig. 7), with sizes varying from 5 to

Table 3
GSD parameters for the experimental slope in JJG.

Regions	Samples	μ	$D_{\mathrm{c}}$
	10 cm before the rainfall	0.040	10.80
	-10 cm after the rainfall	0.036	12.98
R1	-20 cm before the rainfall	0.047	12.44
	20 cm after the rainfall	0.052	12.78
	deposit	0.046	11.94
	10 cm before the rainfall	0.021	10.29
	10 cm after the rainfall	0.019	7.91
R2	20 cm before the rainfall	0.032	10.54
	20 cm after the rainfall	0.041	13.57
	deposit	0.046	17.27

 $1000~(10^{-3}~{\rm m}^3)$ , amounting to approximately  $3.0~{\rm m}^3$ , i.e., more than half the total failure volume. Finally, at the end of the experiment, the slope was left with a 10–30-cm layer stripped off, leaving the scar of a shallow slide.

Fig. 7 also shows the difference in failure activity between regions R1 and R2. All the major failures occurred in R1, accounting for 83% of the total failure volume. The following discussion reveals that the difference is attributable to soil texture, i.e., R1 and R2 have different average GSD parameters:  $\mu$ (R1) = 0.04 and  $\mu$ (R2) = 0.02.

Similar failure sequences occurred in the other experiments, except with different time intervals, failure numbers, and failure magnitudes. It is noted that NJG and JJG have different threshold rainfall intensities, i. e., 45 mm/h in NJG and 27 mm/h in JJG for slides. Moreover, the JJG slope is dominated by slides, whereas the NJG slope is dominated by soil flows of rill erosion. Correspondingly, slides contributed the majority of the total failure volume in JJG, e.g., approximately 79%, 84%, and 83% in experiments J-5, J-6, and J-7, respectively. Conversely, rill erosion failures in NJG accounted for 45% of the total failure volume at 70 mm/h and 61% at 80 mm/h. Table 4 provides a summary of the major data relating to the experiments.

The observations indicate that the coarse-grained characteristic of the JJG slope determines its shallow soil failures, while the fine-grained characteristic of the NJG slope determines that surface flow rills represent the major erosive activity. This qualitatively agrees with phenomena observed in other laboratory-based experiments (e.g., Wang and Sassa, 2003) and implies that soil structure plays a crucial role in slope processes. As indicated in Table 1, the GSD parameters of the two slopes are disparate, with differences much higher than that of the normal variance within a slope. In the study locations, the effects of other landform factors are largely ignorable because the slopes are generally similar, i.e., near to the critical friction angle. In effect, the heterogeneity of the soil leads to the great variety of the observed failures.

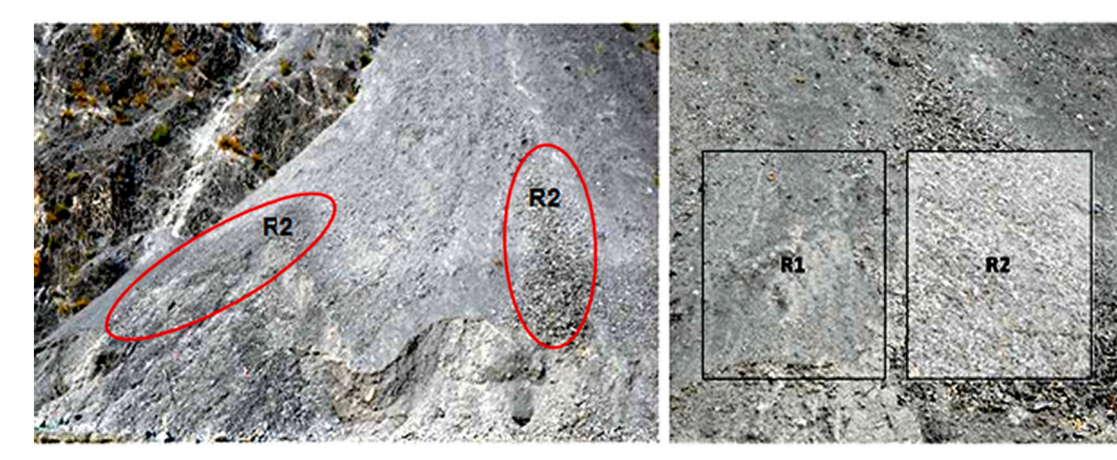


Fig. 6. Slope failure experiment J-7 in JJG.

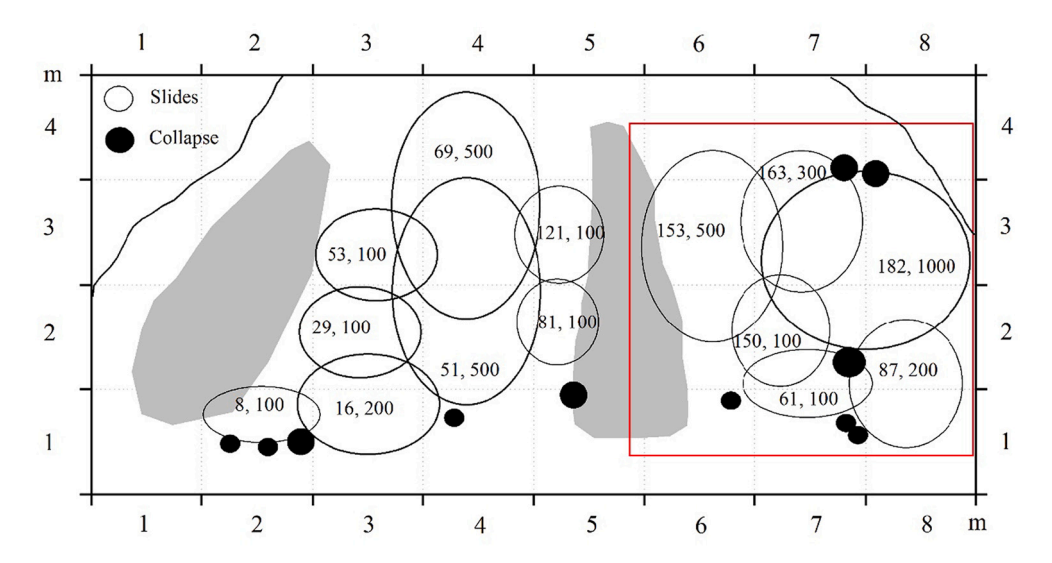


Fig. 7. Spatial distribution of slope failures in experiment J-7 (R1: white region, R2: gray regions).

**Table 4**Summary of soil failures of the experiment.

Valleys	No.	IR	$N_{\rm C}$	$T_{\mathrm{m}}$	$T_{\rm max}$	$M_{\rm max}$	M	$T_1$	
	J-1	12	93	25.54	111	30	998	_	
	J-2	18	92	25.83	95	100	1173	_	
	J-3	27	87	27.14	129	200	1395	35min08s	
JJG	J-4	36	97	24.47	175	500	2305	17min51s	
	J-5	45	141	16.8	61	500	3846	10min16s	
	J-6	54	152	15.79	51	800	5001	10min04s	
	J-7	60	222	10.27	58	1000	5928	7min36s	
	N-1	18	50	48	375	30	439	_	
NJG	N-2	25	55	41.8	323	25	353	_	
	N-3	35	68	32.9	198	70	679	_	
	N-4	45	110	21.6	181	60	1200	31min6s	
	N-5	70	195	11.3	71	500	3587	2min54s	
	N-6	80	150	15.8	146	300	1934	4min35s	

IR: rainfall intensity (mm/h); Nc: failure number;  $T_m$ : mean interval (s);  $T_{max}$ : longest interval (s);  $M_{max}$ : largest failure size ( $10^{-3}$  m<sup>3</sup>); M: total failure amount ( $10^{-3}$  m<sup>3</sup>);  $T_1$ : time of first slide.

## 4. Spatiotemporal characteristics of failure sequences

## 4.1. Statistics of failure sequences

The failures that occur at random in the slope form a sequence that provides a discontinuous supply of material for debris flows and leads to fluctuation of flow surges. For a debris flow, the entire failure sequence rather than any individual failure should be considered because the overall characteristics of the sequence determine the properties of the debris flows. Fig. 8 displays the temporal evolution of the failure sequences that, as discussed later, have several aspects in common associated with the underlying mechanism.

## 4.1.1. Spatial distribution on the slope

The failures are distributed unevenly on the slopes, with some locations having high concentration of failures and other locations having isolated failures. This is because individual collapses and slides are spatially independent and controlled only by local conditions, whereas rill erosion is a cascading process.

## 4.1.2. Temporal intermittency

The failures occurred in succession with time intervals of approximately 20 s (Table 4). It is found that the average interval ( $T_i$ ) decreases exponentially with rainfall intensity (Fig. 9a), and that the number of

failures  $N_c$  (Fig. 9b) increases exponentially with rainfall intensity ( $I_R$ ):

$$T_i = C_T \exp(-k_T I_R) \tag{2}$$

$$N_c = C_N \exp(k_N I_R) \tag{3}$$

where  $C_T$  and  $C_N$  are coefficients, and  $k_T$  and  $k_N$  are exponents, as listed in Table 5.

Moreover, the time interval follows an exponential distribution (Fig. 10), which suggests that the sequence should result from a Poisson process, as discussed later:

$$P(T) \sim exp.(-\lambda T)$$
 (4)

where P(T) is the fraction of failures with time interval longer than T, and  $\lambda$  is the exponent, which is also the intensity of the Poisson process. In definition,  $\lambda$  is the average time interval.

## 4.1.3. Magnitude fluctuation

The failure magnitude fluctuates considerably in the range of  $0.1-500\ (10^{-3}\ m^3)\ (Fig.\ 8)$ , and large or small failures occur unexpectedly across the slope under given soil and rainfall conditions. The degree of fluctuation implies that extremely large failures might occur under ordinary conditions, while small failures might occur under conditions of very high rainfall intensity.

Although individual failures cannot be associated with specific rainfall intensity, the failure magnitude is generally well correlated with rainfall intensity. It is found that the average magnitude of a failure ( $M_c$ ) increases exponentially with rainfall intensity (Fig. 11a):

$$M_c = C_M \exp.(k_M I_R) \tag{5}$$

which provides an estimate of the total volume of a failure at a given value of  $I_{\rm R}$ , as expressed by (Fig. 11b):

$$M_{\rm S} = N_c M_c = K \exp(k_{\rm s} I_R) \tag{6}$$

where  $K = C_N C_M$  and  $k_s = k_M + k_N$ , are empirical coefficients that vary with slope and can be determined by experiment. The parameters of the relationship between slope failure and rainfall intensity are listed in Table 5. Rainfall intensity imposes an "exponential effect" on the failures that reflects the nonlinearity of slope processes.

Moreover, failure magnitude satisfies the power law distribution (Fig. 12):

$$P(\rangle M) = BM^{-b} \tag{7}$$

where P(>M) is the fraction of failures with volume bigger than M, B is a

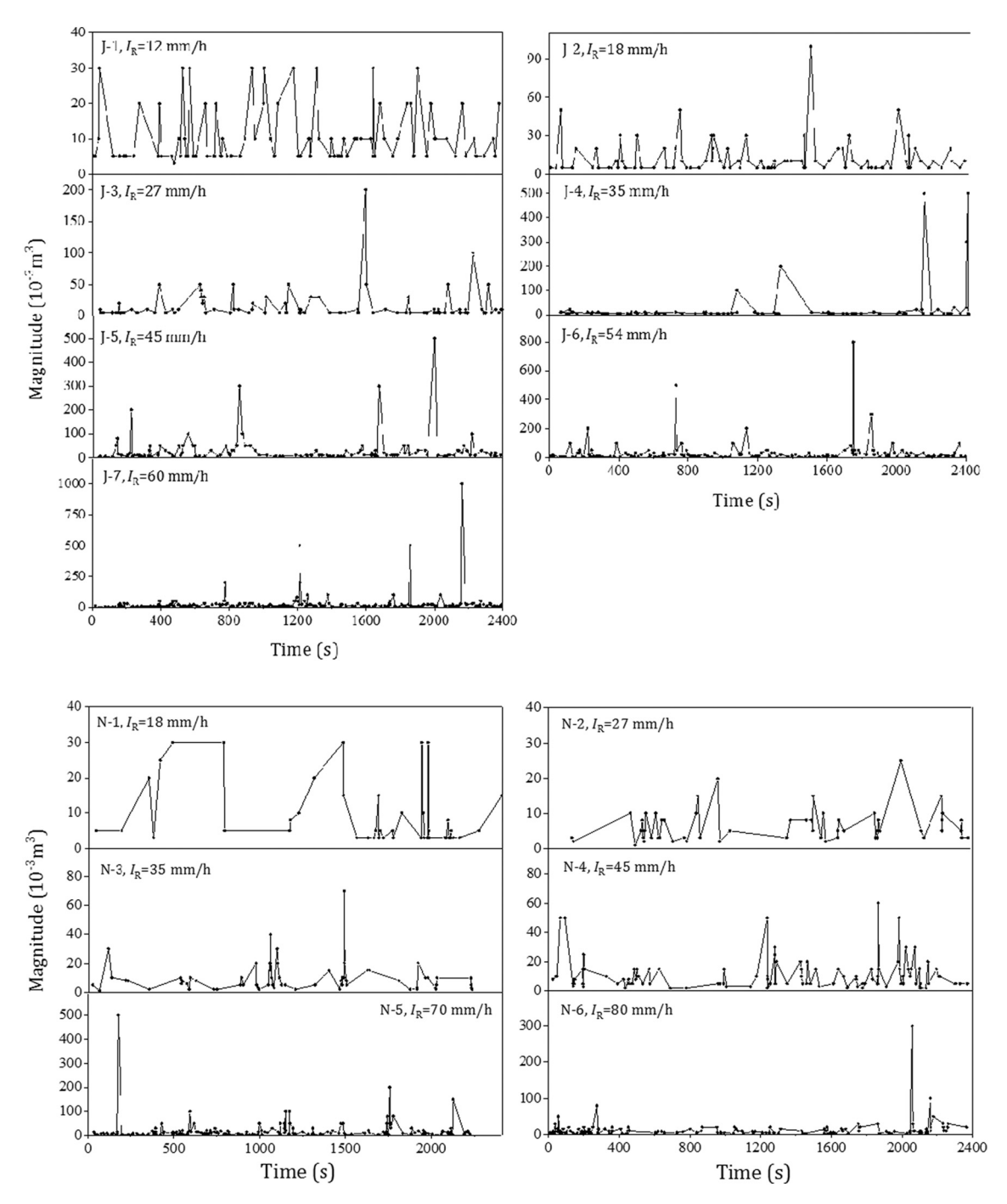


Fig. 8. Failure sequences of all experiments.

coefficient, and b is the power exponent.

The power law has generally been observed in relation to landslides (e.g., Malamud et al., 2004; Katz and Aharonov, 2006), suggesting that a slope failure system is similar to an avalanche system, which can be exemplified by a sandpile model that presents a power law magnitude–frequency relationship associated with the mechanism of self-organized criticality (Bak et al., 1988; Pierre, 1991; Turcotte, 1997; Hergarten, 2003). However, self-organized criticality is more a philosophical framework for an avalanche than a technical representation of slope failure. In the self-organized criticality paradigm, the system is governed by the repose angle and the system adjusts its stationary state through avalanches. In the case of a soil slope, the failure process is triggered by rainfall through water–soil interaction, where both the external factor of rainfall and the intrinsic factor of the granular

structure of the soil are crucial.

## 4.2. Characteristics of failure sequences as a time series

The systematic features of the failure sequences are considered, taking each as a time series, to reveal the nature of failure. The Pearson, Kendall, and Spearman coefficients (Fieller et al., 1957; Kendall and Stuart, 1983) between failure size and failure interval were calculated to describe their correlation (Table 6). In most cases, the magnitude of the coefficients (either negative or positive) appears small, suggesting that failure does not develop with time. Only at low rainfall intensity is weak correlation found. This implies that the entire failure process does not depend on local variation of influencing factors, e.g., pore water pressure or infiltration. In this respect, shallow failures appear distinct from

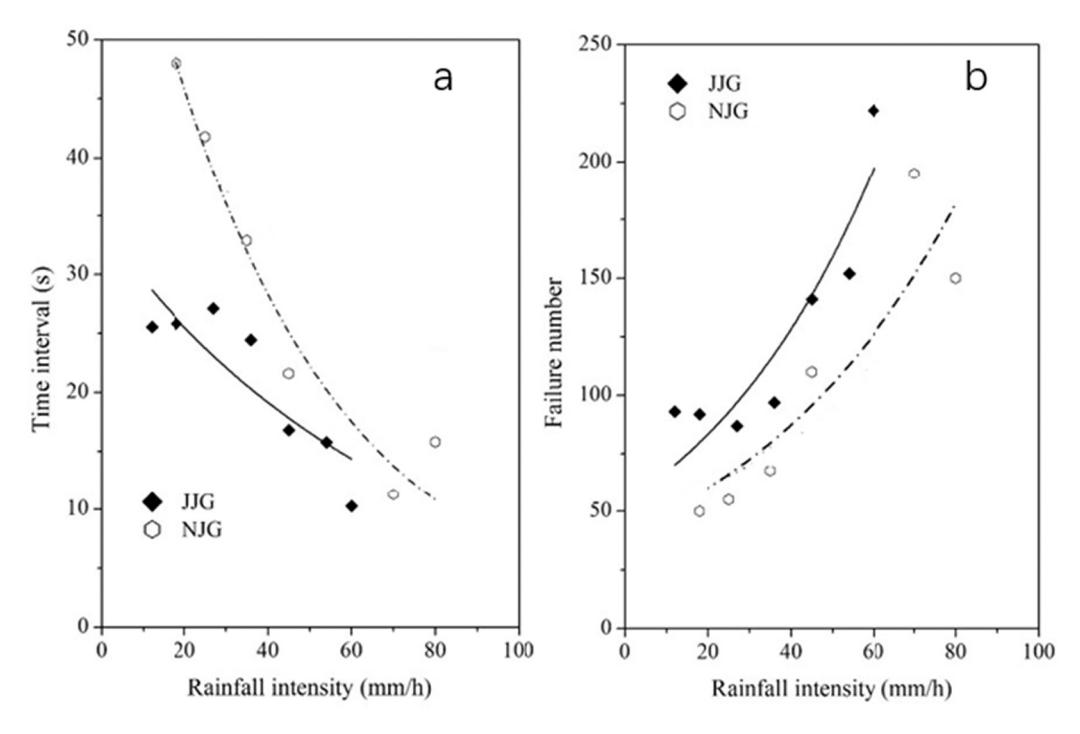
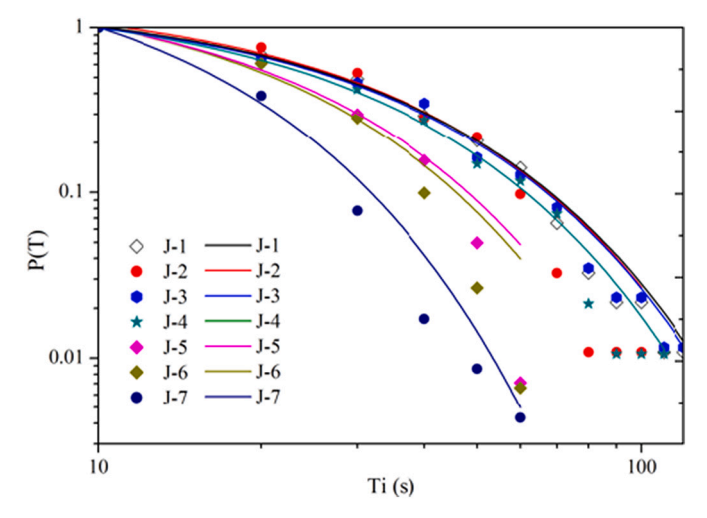


Fig. 9. Relation of (a) time interval and (b) failure number with rainfall intensity.

**Table 5**Parameters of exponential relationship between slope failures and rainfall intensity.

Slope	Time interval		Failure r	Failure number		Average failure size		Total failure volume				
	$C_T$	$k_T$	$R^2$	$C_N$	$k_N$	$R^2$	$C_M$	$k_M$	$R^2$	$C_{\rm t}$	$k_s$	$R^2$
JJG	45.1	0.022	0.9156	53.3	0.021	0.8594	8.94	0.022	0.8854	568.4	0.040	0.9820
NJG	67.4	0.022	0.8842	34.8	0.021	0.8965	12.3	0.004	0.9014	216.5	0.033	0.8435



 ${f Fig.~10.}$  Exponential distribution of time intervals of failures (taking JJG as an example).

large landslides that evolve with temporal processes of rainfall and soil mechanics (Lee, 1984; William, 2004). However, the increasing coefficient of variance with rainfall means that intense rainfall (intensity) facilitates extreme large failures.

Furthermore, we consider the memory feature of a sequence using the Hurst exponent (Hurst et al., 1965; McCauley et al., 2007) with the Augmented Dickey–Fuller test and the Mann–Kendall Trend test (Table 7). The Hurst exponent is mostly slightly larger than 0.50, suggesting again the randomness of the sequence, while the weak correlation and trend (or long-term memory) simply correspond to the rapid decay of the autocorrelation coefficient, as shown in Fig. 13.

Time series analysis indicates that a failure sequence that comprises primarily random uncorrelated individual failures is independent of rainfall conditions. Therefore, the underlying mechanism of a sequence should be rooted in the field of randomness rather than the dynamics governing individual failures. The following illustrates how a failure sequence is the result of randomness attributable to the spatial heterogeneity of the slope soil.

## 5. Mechanism of a discontinuous failure sequence

## 5.1. Spatial heterogeneity of the slope soil

Discontinuous, fluctuating, and scattered failures cannot be ascribed to any single landsliding mechanism, and the spatiotemporal characteristics presented by the sequences reflect the random nature of the failures.

As observed in the experiments, various failures are rooted in the randomness of the soil texture. Collapses represent granular aggregate falling off a slope, attributable mainly to reduction of friction following lubrication by rainfall; thus, no water–soil interaction or destruction of soil structure is involved. Collapses are therefore completely random and can occur under any rainfall conditions. Slides and rill erosion reflect destruction of the soil structure under the effects of rainfall infiltration and surface flows, respectively, in association with variations of soil mechanical parameters such as pore water pressure p,

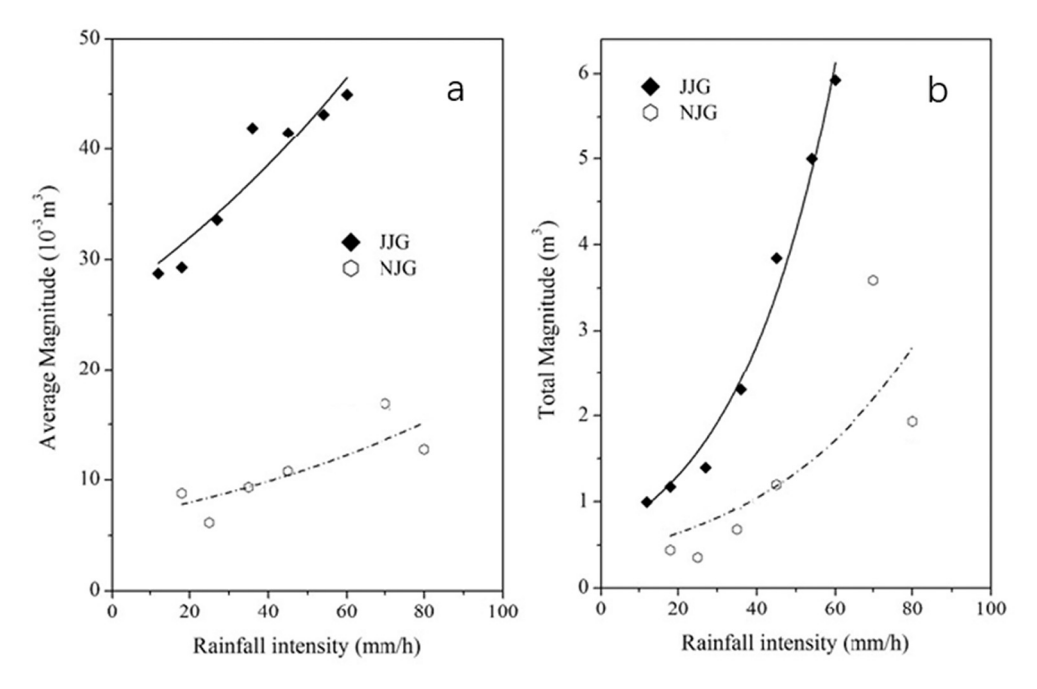
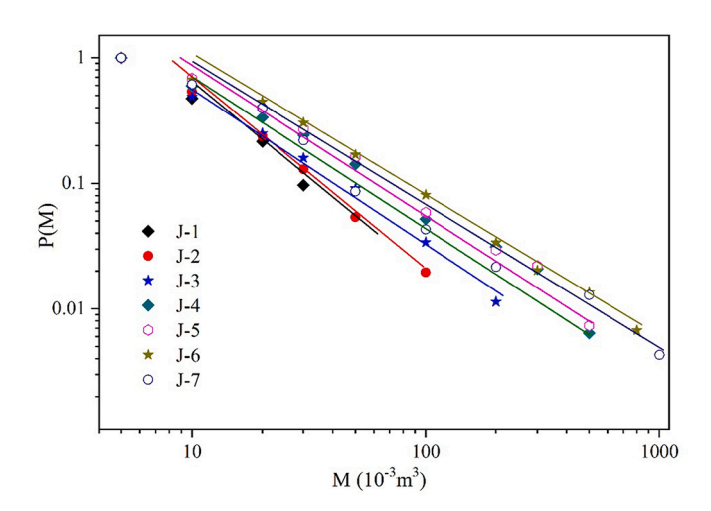


Fig. 11. Relation between (a) average failure magnitude and (b) total failure magnitude with rainfall intensity.



 $\begin{tabular}{ll} {\bf Fig.~12.~Magnitude-frequency~relationship~of~slope~failure~(taking~JJG~as~an~example).} \end{tabular}$ 

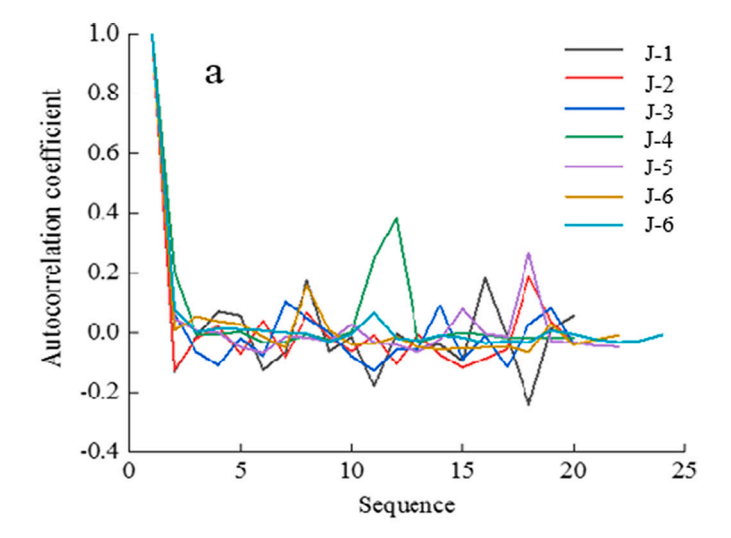
cohesion C, and effective stress  $\sigma$ . Despite the variety of failure mechanisms, these processes are rooted in the spatial heterogeneity of the soil. In previous related studies, soil heterogeneity has been described using a Monte Carlo simulation (*Griffiths* and *Fenton*, 1993, 2004),

**Table 7**Statistical values of slope failure sequences.

		•		
Valley	experiments	Hurst exponent	ADF test (P)	Mann-Kendall Trend test
	J-1	0.5368	0.01	upward, not obvious
	J-2	0.482	0.01	upward, not obvious
	J-3	0.519	0.01	downward, not obvious
JJG	J-4	0.574	0.015	upward, not obvious
	J-5	0.5071	0.01	upward, not obvious
	J-6	0.5589	0.01	upward, not obvious
	J-7	0.5757	0.01	upward, obvious
	N-1	0.6797	0.01	downward, not obvious
	N-2	0.5304	0.015	upward, not obvious
	N-3	0.634	0.22	downward, not obvious
NJG	N-4	0.637	0.01	downward, not obvious
	N-5	0.5557	0.01	upward, not obvious
	N-6	0.5819	0.01	upward, not obvious

**Table 6**Correlation between rainfall and failure sequences.

Valley	Experiments	Rainfall		CV(%)	Correlation coe	Correlation coefficient			
		Intensity (mm/h)	ntensity (mm/h) Amount		Pearson	Kendall	Spearman		
			(mm)						
	J-1	12	7.92	74.78	0.0388	0.052	0.0662		
	J-2	18	11.93	108.48	-0.0083	0.012	0.0175		
	J-3	25	16.6	160.64	0.05	-0.0139	-0.0172		
JJG	J-4	36	23.9	330.69	-0.1318	-0.0029	-0.0035		
	J-5	45	29.9	221.25	0.123	0.147	0.1966		
	J-6	54	35.94	250.71	0.0131	0.0061	0.0128		
	J-7	60	40	318.56	-0.046	0.0426	0.0542		
	N-1	18	12	99.8	0.3163	0.1905	0.2492		
	N-2	25	16.6	73.73	0.2163	0.0589	0.0882		
NIC	N-3	35	21.69	106.09	-0.1089	-0.1081	-0.1466		
NJG	N-4	45	29.69	101.56	-0.022	0.0679	0.0909		
	N-5	70	43.26	227.85	-0.0763	-0.0405	-0.0542		
	N-6	80	52.62	206.73	0.0402	0.1063	0.1432		



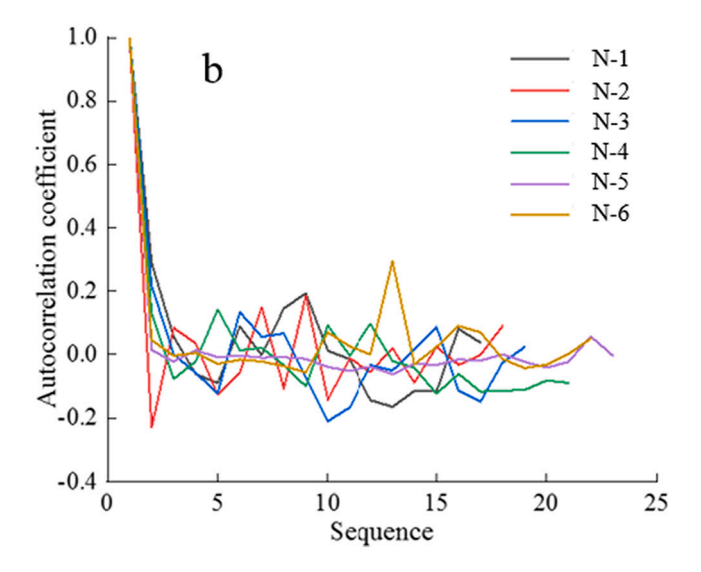


Fig. 13. Autocorrelation coefficients of the slope failure sequences.

which provides a distribution of the safety factor associated with some failure models (e.g., Hicks et al., 2008, 2014), and can predict a single landslide based on the safety factors. Consideration of a failure sequence requires representation of both the fluctuation of failure magnitude and the separation of individual failures in space and time. The GSD is a natural random variable that can provide such representation.

As indicated by the soil samples, GSD parameters vary remarkably from point to point across a slope, which means that a soil body acts as a granular field characterized by the parameters  $\mu$  and  $D_c$ . As soil properties depend mainly on the fine-grained content (represented by  $\mu$ ) (Wang and Sassa, 2003; Cui et al., 2017; Guo and Cui, 2020), we consider only the  $\mu$  field. Soil samples and field surveys revealed that the values of  $\mu$  across the slope satisfy the Weibull distribution:

$$p(\mu) = Weib(\lambda_{\mu}, k) = \frac{\lambda_{\mu}}{k} \left(\frac{\mu}{\lambda}\right)^{k-1} exp\left(-\left(\mu/\lambda_{\mu}\right)^{k}\right)$$
 (8)

where  $\lambda_{\mu}$  and k are the scale and shape parameter, respectively, both appear to decrease with slope gradient. As the average  $<\mu \geq \lambda\Gamma(1+1/k)$ , a steep slope might take a small value of  $\mu$  on average. Therefore, the GSD parameter provides a natural index for soil slope. Fig. 14 shows the Weibull distribution of  $\mu$  for the soil of two slopes in JJG. It can be seen that slope A has a much higher fine-grained content than slope B, with average values of  $\mu$  of 0.037 and 0.014, respectively.

In response to GSD, other soil properties also vary from point to point

across a slope. Specifically, the parameters primarily responsible for slope stability, i.e., cohesion C and friction angle  $\varphi$ , are distributed randomly in a soil slope. A series of experiments conducted under various conditions indicated that both parameters are associated with GSD in a power law form (Gou et al., 2015):

$$C \sim A_c \,\mu^{\alpha} \text{ and } \varphi \sim A_{\varphi} \, D_c^{-\beta}$$
 (9)

The Weibull distribution has the merit of power law invariance, meaning that when  $\mu$  satisfies the Weibull distribution Weib $(\lambda_{\mu}, k_{\mu})$ , the variable as a power law function of  $\mu$  also satisfies the Weibull distribution. It can be determined that C follows

$$p(C) = Weib\left(A_{\mu}\lambda_{\mu}^{\alpha}, \frac{k_{\mu}}{\alpha}\right) \tag{10}$$

Similarly,

$$p(\varphi) = Weib\left(A_{\varphi}\lambda_{D_c}\beta, \frac{k_{D_c}}{\beta}\right) \tag{11}$$

when  $D_c$  satisfies Weib ( $\lambda_D$ ,  $k_D$ ).

Thus, the soil strength  $\tau = C + \sigma \tan \varphi$  actually varies with GSD as.

$$\tau(\mu, D_{\rm c}) = C(\mu, D_{\rm c}) + \sigma tan\varphi(\mu, D_{\rm c}) \tag{12}$$

Considering effective stress  $\sigma$  as a normal variable that satisfies the normal distribution Norm(45, 1) (with mean stress of 45 KPa and variance of 1 KPa, according to general cases in reality), and based on our experiment results, i.e.,  $p(C) \sim \text{Weib}(15, 2.5)$  and  $p(1/\varphi) \sim \text{Weib}(0.03, 18)$ , the random fluctuation of stress for a soil slope can be obtained (Fig. 15), which again satisfies Weib(47.17, 7.52) (Fig. 16).

## 5.2. Origin of intermittency and fluctuation

As shown in Table 4, the time after rainfall before the first slide occurs varies considerably and depends on both the rainfall intensity and the soil structure. In the case of a monodispersed granular aggregate, the dilation effect might introduce intermittency in avalanches (Bagnold, 1966; Pierre, 1991) when the aggregate is denser than a specific critical density. Experiments on soils (e.g., Iverson et al., 2000) also indicate that dilation or contraction effects lead to catastrophic landslide or slow failure, respectively, at different time scales. The time scale of the buildup and dissipation of pore water pressure is assumed to take a dominant role in the intermittent process (Iverson, 1997; Iverson et al., 1997, 2000; Guo et al., 2016a).

For the present case of very shallow failures, changes in granular structure are obviously effective, and changes in porosity (dilation or contraction) are determined by the varying GSD parameters, which define the characteristic porosity as follows (Li et al., 2013):

$$\varepsilon = 1 - \left(D_0/D_{\rm m}\right)^{\mu} \tag{13}$$

where  $D_0$  and  $D_{\rm m}$  define the lower and upper limits, respectively, of the scaling range for the grain aggregate, i.e., the range within which the power law distribution holds ( $P(D) \sim D^{-\mu}$ ), which is approximately 0.001–1.0 mm (Li et al., 2013). Then, the porosity variation due to migration of fine grains attributable to infiltration can be expressed as follows:

$$|\Delta\varepsilon| = (1 - \varepsilon)|\operatorname{Ln}(D_0/D_{\mathrm{m}})|\Delta\mu \text{ or}|\Delta\varepsilon/(1 - \varepsilon)| = |\operatorname{Ln}(D_0/D_{\mathrm{m}})|\Delta\mu$$
(14)

It is found that the loss of fine grains increases nearly exponentially with rainfall intensity (Zhou et al., 2012), meaning that  $\Delta\mu\sim \exp(I_R)$ . Thus, changes in the soil are sensitive to GSD and rainfall intensity. As experiments proved, failure is sensitive to the initial porosity. A slope soil with initial porosity  $\varepsilon=0.41$  or  $\varepsilon=0.46$  (i.e.,  $\mu=0.025$  or 0.03) might result in a catastrophically accelerating landslide or intermittent mass creep (e.g., Iverson et al., 2000). Thus, the sensitivity of failure to initial porosity reduces to sensitivity to the GSD exponent  $\mu$ .

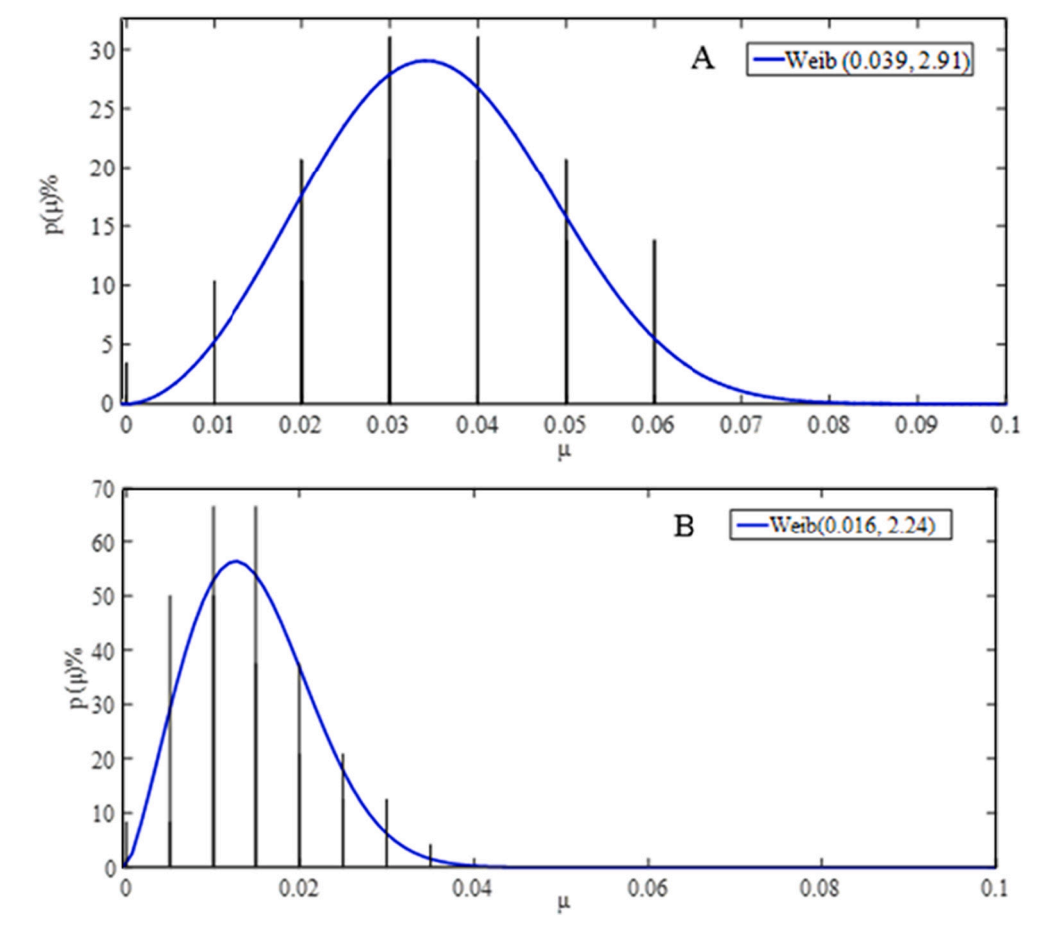


**Fig. 14.** Weibull distribution of GSD parameter  $\mu$  for two slopes in JJG.

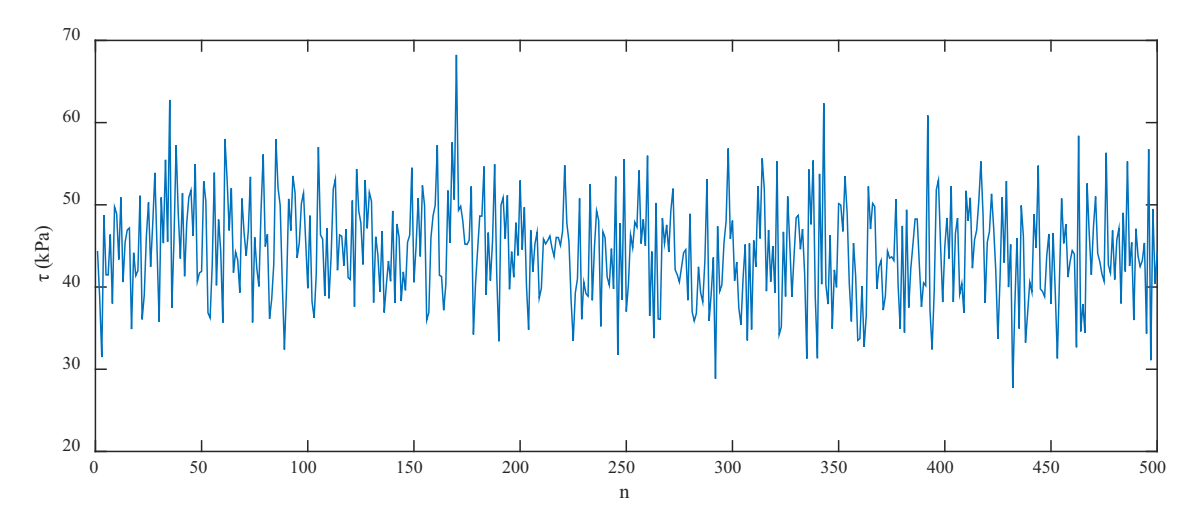


Fig. 15. Stress fluctuation in a soil slope.

The ratio of the time scale of the generation and diffusion of pore water pressure (i.e.,  $T_{pg}$  and  $T_{pd}$ , respectively) can be defined as follows (Iverson, 1997):

$$R_T = T_{\rm pg}/T_{\rm pd} = K_{\rm p}E/\eta u \delta \tag{15}$$

where  $K_p$  is the hydraulic permeability (m<sup>2</sup>), E is Young's compression modulus (Pa), u is the velocity of intergranular sliding (m/s),  $\eta$  is the dynamical viscosity of pore fluid (Pa.s), and  $\delta$  is the characteristic length (m). Here,  $\delta$  can be taken as the characteristic size  $D_c$  because it

represents an essential unit of soil covering grains of all sizes. Experiments indicate that permeability  $K_{\rm C}$  (= $K_{\rm p}/g/\eta$ ) =  $-\log(\mu)$  (Xie, 2014), and that E and u can be considered to vary little within the small area of failure. Then, Eq. (15) reduces to  $R_T \sim K_{\rm p}/D_{\rm C} \sim \log(1/\mu)/D_{\rm c}$ , which is simply determined by the GSD parameters. This implies that fine soils are more susceptible to pore water pressure buildup, while such pressure is dissipated rapidly in coarse soils. For example, in the JJG experiments, the slope shows considerable difference in the initial value of parameter  $\mu$  between R1 and R2 (Table 3). The fine-grained content in R1 is higher

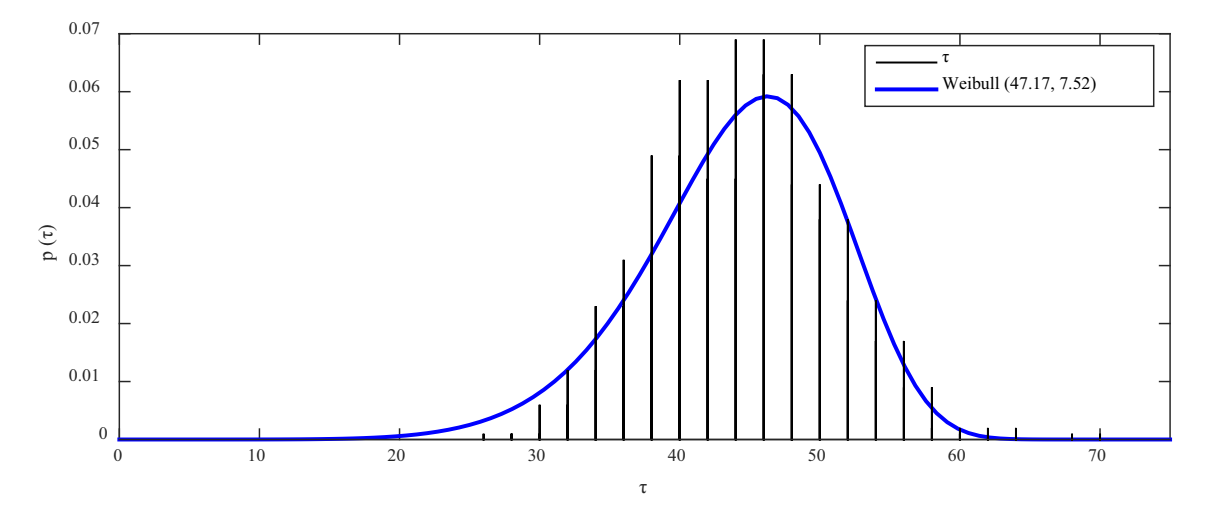


Fig. 16. Weibull distribution of strength stress in a soil slope.

than in R2 and thus pore water pressure buildup occurs more easily in R1. Consequently, the number and quantity of failures are much higher in R1. Because  $R_{\rm T}$  varies with  $(\mu, D_{\rm c})$ , it is responsible for the failures at the various sites across the slope.

In summary, the spatial heterogeneity of soil characterized by the point-to-point variation of GSD parameters is the fundamental cause for the discontinuous and fluctuating occurrence of failures. The variation of  $\mu$  governs the mode and magnitude of the failures, and the amplitude of the variation of  $\mu$  ( $\Delta\mu$ ) determines the fluctuation of failure occurrence.

## 6. Discussion: implication of failures to debris flow surges

Our experiments revealed the collective behavior of slope failures, and established the statistical characteristics of failure sequences. It was proven that the spatial heterogeneity of soil determines the variety of slope processes, and that this can be reduced to the variation of GSD parameters ( $\mu$ ,  $D_c$ ).

As observed in relation to our experiments, the primary concern regarding slope failure is not the dynamics of individual landslides but the phenomenon of a failure sequence. The entirety of a failure sequence (the time and magnitude series of failure) illustrates a vivid scenario for such a slope process. In particular, this provides a new mechanism for the occurrence of debris flow surges. As shown in Fig. 17 (experiment N-5, rainfall: 70 mm/h), slope failures can result in several separate flow surges that in this case involved the following three processes.

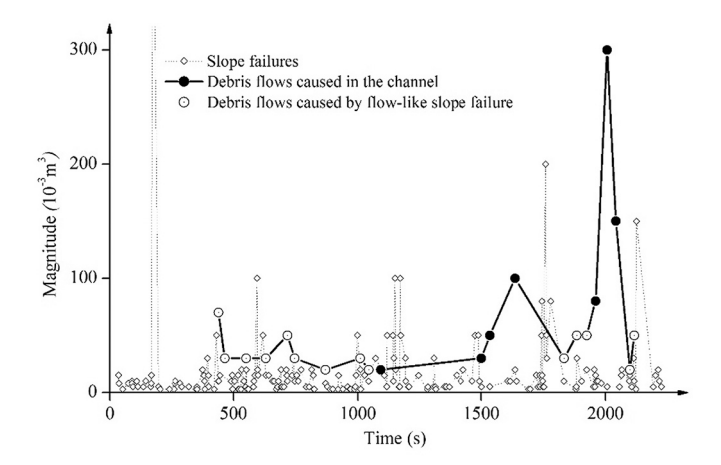


Fig. 17. Surges formed by slope failures (experiment N-5, rainfall: 70 mm/h).

- 1) A small failure reaches the channel and mixes with flowing water to form a flow surge with low sediment concentration.
- Flow-like failures (mainly from rill erosion) move off the slope and continue to flow and form debris flows with various concentrations.
- 3) A large failure is deposited in the channel and forms a small blockage, which is then eroded either partially or en masse, depending on the impounded water or the discharge of the water flow, to form surges.

Although the experiments in this study were restricted to small areas, the scenarios of the failures and tributary surges are generally observed in debris flow valleys, and the random confluence of tributary flows results in mainstream surges. Observations in JJG have confirmed that the surge sequence presents spatiotemporal characteristics similar to those of the slope failure sequence, e.g., intermittency, fluctuation, and magnitude distribution (e.g., Liu et al., 2008, 2009; Li et al., 2015).

## 7. Conclusions

Several groups of shallow soil failure experiments were conducted on slopes in debris flow source areas, which provided a complete failure sequence scenario involving various regimes. Details of the specific findings are as follows.

- 1) Individual failures occur randomly and intermittently with fluctuation of up to three orders of magnitude. The failure magnitude satisfies the power law distribution, the time interval satisfies the exponential distribution, and the distribution parameters are related specifically to rainfall intensity.
- 2) The slope process appears in the form of a failure sequence, which comprises random uncorrelated individual failures, and is independent of rainfall conditions. The randomness can be ascribed to the spatial heterogeneity of soil characterized by the GSD parameters ( $\mu$ ,  $D_c$ ). The point-to-point variation of soil properties ( $\mu$ ,  $D_c$ ) leads to dramatic changes in the distribution of strength, infiltration, and pore water pressure generation that result in the variety of failures distributed randomly across the slope.
- 3) Discontinuous failures translate into separate debris flow surges in the tributaries, thereby providing a scenario for surge formation in the mainstream flow of the valley. It is suggested that surges in the mainstream channel result from cascading development of tributary surges, and that the spatiotemporal characteristics observed in mainstream surges are rooted in the sources of slope failures.

In summary, the experiments conducted in this study revealed the spatiotemporal characteristics of slope failures, and provided a vivid scenario for failure sequences that present a characteristic of randomness, which can be ascribed to the spatial heterogeneity of the soil that can ultimately be explained in terms of GSD parameters.

#### Credit author statement

Xiaojun Guo: Conceptualization, Methodology, Experiment, Data processing and Writing.

Yong Li: Conceptualization, Reviewing and Editing.

Peng Cui: Conceptualization.

Yan Yan: Experiment, and Data processing.

Baoliang Wang: Experiment. Jun Zhang: Data processing.

## **Declaration of Competing Interest**

None

## Acknowledgements

This study was supported by the Major Program of National Natural Science Foundation of China (Grant Nos. 41790432, 41977257); the Strategic Priority Research Program of the Chinese Academy of Sciences (Grant No. XDA23090202); and the Joint Research Project of Sichuan Provincial Highway Planning, Survey and Design Research Institute Co., Ltd (2021-A-08). We thank James Buxton MSc, from Liwen Bianji (Edanz) (www.liwenbianji.cn), for editing the English text of a draft of this manuscript.

#### References

- Baecher, G.B., Christian, J.T., 2005. Reliability and Statistics in Geotechnical Engineering. John Wiley & Sons Ltd., Chichester, England.
- Bagnold, R.A., 1966. Shearing and dilatation of dry sand and singing mechanism. Proc. R. Soc. London, Ser. A 295 (1442), 219–232.
- Bak, P., Tang, C., Wiesenfeld, K., 1988. Self-organized criticality. Phys. Rev. A 38, 364–374.
- Cui, P., Chen, X.Q., Wang, Y.Y., Hu, K.H., Li, Y., 2005. Jiangjia Ravine debris flows in south-western China. In: Jakob, M., Hungr, O. (Eds.), Debris-Flow Hazards and Related Phenomena. Springer Berlin Heidelberg, Praxis, pp. 65–594.
- Cui, Y.F., Zhou, X.J., Guo, C.X., 2017. Experimental study on the moving characteristics of fine grains in wide grading unconsolidated soil under heavy rainfall. J. Mt. Sci. 14 (3), 417–431.
- Feng, F., Li, X.B., Rostami, J., Peng, D.X., Li, D.Y., Du, K., 2019. Numerical investigation of hard rock strength and fracturing under polyaxial compression based on Mogi-Coulomb failure criterion. Int. J. Geomech. 19 (4), 04019005.
- Fieller, E.C., Hartley, H.O., Pearson, E.S., 1957. Tests for rank correlation coefficients. I. Biometrika 44, 470–481.
- Gou, W.C., Li, Y., Wang, B.L., Liu, D.C., 2015. Relationship between granularity of debris flow deposit and the strength. Sci. Technol. Eng. 15 (35), 136–140 (In Chinese).
- Griffiths, D.V., Fenton, G.A., 1993. Seepage beneath water retaining structures founded on spatially random soil. Géotechnique 43 (4), 577–587.
- Griffiths, D.V., Fenton, G.A., 2004. Probabilistic slope stability analysis by finite elements. J. Geotech. Geoenviron. 130 (5), 507–518.
- Guo, C.X., Cui, Y.F., 2020. Pore structure characteristics of debris flow source material in the Wenchuan earthquake area. Eng. Geol. 267, 105499.
- Guo, X.J., Li, Y., Cui, P., Zhao, W.Y., Jiang, X.Y., Yan, Y., 2016a. Discontinuous slope failures and pore-water pressure variation. J. Mt. Sci. 13 (1), 116–125.
- Guo, X.J., Cui, P., Li, Y., Ma, Li, Ge, Y.G., William, B.M., 2016b. Intensity-duration threshold of rainfall triggering debris flows in Wenchuan earthquake area, China. Geomorphology 263, 208–216.
- Guo, X.J., Li, Y., Cui, P., Yan, H., Zhuang, J.Q., 2020. Intermittent viscous debris flow formation in Jiangjia Gully from the perspectives of hydrological processes and material supply. J. Hydrol. 589, 125184.
- Hergarten, S., 2003. Landslides, sandpiles, and self-organized criticality. Nat. Hazards Earth Syst. Sci. 3, 505–514.

- Hicks, M.A., Chen, J., Spencer, W.A., 2008. Influence of spatial variability on 3D slope failures. In: Brebbia, C.A., Beriatos, E. (Eds.), Proceedings of the 6th International Conference on Computer Simulations in Risk Analysis and Hazard Mitigation, Cephalonia, Greece, pp. 335–342.
- Hicks, M.A., Nuttall, J.D., Chen, J., 2014. Influence of heterogeneity on 3D slope reliability and failure consequence. Comput. Geotech. 61, 1198–1208.
- Hungr, O., Leroueil, S., Picarelli, L., 2014. The Varnes classification of landslide types, an update. Landslides 11 (2), 167–194.
- Hurst, H.E., Black, R., Sinaika, Y.M., 1965. Long-Term Storage in Reservoirs: An Experimental Study. Constable, London.
- Iverson, R.M., 1997. The physics of debris flows. Rev. Geophys. 35 (3), 245–296.
- Iverson, R.M., Reid, M.E., LaHusen, R.G., 1997. Debris-flow mobilization from landslides. Annu. Rev. Earth Planet. Sci. 25, 85–138.
- Iverson, R.M., Reid, M.E., Iverson, N.R., LaHusen, R.G., Logan, M., Mann, J.E., Brien, D. L., 2000. Acute sensitivity of landslide rates to initial soil porosity. Science 290, 513–516.
- Katz, O., Aharonov, E., 2006. Landslides in vibrating sand box: what controls types of slope failure and frequency magnitude relations? Earth Planet. Sci. Lett. 247, 280–294.
- Kendall, M., Stuart, A., 1983. The Advanced Theory of Statistics. Vol. 3: Distribution Theory. Griffin, London, pp. 410–414.
- Lee, I.K., 1984. In: Soil mechanics, Finkl, C. (Eds.), Applied Geology. Encyclopedia of Earth Sciences Series, vol 3. Springer, Boston, MA.
- Li, Y., Zhou, X.J., Su, P.C., Kong, Y.D., Liu, J.J., 2013. A scaling distribution for grain composition of debris flow. Geomorphology 192, 30–42.
- Li, Y., Liu, J.J., Guo, X.J., Su, F.H., Xie, J., Wang, B.L., 2015. Relationship between grain composition and debris flow characteristics: a case study of the Jiangjia Gully in China. Landslides 12 (1), 19–28.
- Li, Y., Huang, C.M., Wang, B.L., Tian, X.F., Liu, J.J., 2017. A unified expression for grain size distribution of soils. Geoderma 288, 105–119.
- Liu, J.J., Li, Y., Su, P.C., Cheng, Z.L., 2008. Magnitude–frequency relations in debris flow. Environ. Geol. 55, 1345–1354.
- Liu, J.J., Li, Y., Su, P.C., Cheng, Z.L., Cui, P., 2009. Temporal variation of intermittent surges of debris flow. J. Hydrol. 365, 322–328.
- Malamud, B.D., Turcotte, D.L., Guzzetti, F., Reichenbach, P., 2004. Landslide inventories and their statistical properties. Earth Surf. Process. Landf. 29, 687–711.
- McCauley, J.L., Gunarame, G.H., Bassler, K.E., 2007. Hurst exponents, Markov processes, and fractional Brownian motion. Physica A 379, 1–9.
- Mori, H., Chen, X.Y., Leung, Y.F., Shimokawa, D., Lo, M.K., 2020. Landslide hazard assessment by smoothed particle hydrodynamics with spatially variable soil properties and statistical rainfall distribution. Can. Geotech. J. 57 (12), 1953–1969.
- Phoon, K.K., Kulhawy, F.H., 1999. Characterization of geotechnical variability. Can. Geotech. J. 36 (4), 612–624.
- Pierre, E., 1991. Analysis of the statistics of sandpile avalanches using soil-mechanics results and concepts. Phys. Rev. A 43, 2720–2740.
- Sharpe, C.F.S., 1938. Landslides and Related Phenomena. Columbia University Press, NY, p. 137.
- Turcotte, D.L., 1997. Fractals and Chaos in Geology and Geophysics, 2nd edn. Cambridge University Press, Cambridge, p. 398.
   Uzielli, M., Vannucchi, G., Phoon, K.K., 2005. Random field characterisation of stress-
- nomalised cone penetration testing parameters. Géotechnique 55 (1), 3–20.
- Vanmarcke, E.H., 1977. Probabilistic modeling of soil profiles. J. Geotech. Eng. Div. ASCE 103 (GT11), 1227–1246.
- Vanmarcke, E.H., 1980. Probabilistic stability analysis of earth slopes. Eng. Geol. 16 (1–2), 29–50.
- Vanmarcke, E.H., 1983. Random Fields: Analysis and Synthesis. MIT Press, Cambridge, MA.
- Varnes, D., 1978. Slope movement types and processes. In: Schuster, R.L., Krizek, R.J. (Eds.), Landslides, Analysis and Control, special report 176: Transportation Research Board. National Academy of Sciences, Washington, DC, pp. 11–33.
- Wang, G.H., Sassa, K., 2003. Pore-pressure generation and movement of rainfall-induced landslides: effects of grain size and fine-particle content. Eng. Geol. 69, 109–125.
   William, P., 2004. Soil Mechanics. Routledge, London.
- Xiao, S., Guo, W.D., Zeng, J.X., 2018. Factor of safety of slope stability from deformation energy. Can. Geotech. J. 55 (1), 296–302.
- Xie, J., 2014. Stability controlling of soil slope under excavating of oil and gas pipeline trench. Master degree thesis of University of Chinese Academy of Sciences, Beijing (in Chinese).
- Yan, Y., Cui, P., Guo, X.J., Ge, Y.G., 2016. Trace projection transformation: a new method for measurement of debris flow surface velocity fields. Front. Earth Sci. 10 (4), 761–771.
- Zhou, X.J., Cui, P., Jia, S.T., Li, Y., 2012. Flume test study on the movement of fine grains based on orthogonal design. J. Sichuan Univ. (Engineering Science Edition) 44 (Z1), 83–88 (in Chinese).